

# Influence of shallow core-level hybridization on the electronic structure of post-transition-metal oxides studied using soft X-ray emission and absorption

Cormac McGuinness, Cristian B. Stagarescu, Philip J. Ryan,\* James E. Downes, Dongfeng Fu, and Kevin E. Smith<sup>†</sup>  
*Department of Physics, Boston University, 590 Commonwealth Avenue, Boston, Massachusetts 02215, USA*

R. G. Egdel

*Inorganic Chemistry Laboratory, Oxford University, South Park Road, Oxford OX1 3QR, United Kingdom*

(Received 19 February 2003; revised manuscript received 12 June 2003; published 20 October 2003)

The influence of shallow core-level hybridization on the electronic structure of the post-transition metal oxides ZnO, CdO,  $\text{In}_2\text{O}_3$ , and  $\text{SnO}_2$  has been investigated using high-resolution soft x-ray emission and absorption spectroscopies. Synchrotron radiation excited O  $K_\alpha$  emission spectra provide a direct measure of the O  $2p$  partial density of states and shallow core-level hybridization for this series of transparent conducting materials and reveal significant mixing of O  $2p$  and shallow-core metal  $d$  states for ZnO, CdO, and  $\text{In}_2\text{O}_3$ . The experimental data are compared with local density approximation and tight-binding band structure calculations and with previous experimental determinations of direct and indirect band gaps. Rocksalt CdO, bixbyite  $\text{In}_2\text{O}_3$ , and rutile  $\text{SnO}_2$  all adopt structures with metal cations in sites with locally centrosymmetric coordination. This prevents hybridization of O  $2p$  states with metal  $4d$  states at the zone center, but mixing away from  $\Gamma$  leads to indirect band gaps for CdO and  $\text{In}_2\text{O}_3$ . A revised value for the lowest indirect band gap in CdO is proposed and the overall trends in the band gap are discussed in terms of the separation between O  $2p$  and metal  $4d$  states. The experimental investigation has been extended to study the effects of Sn doping in  $\text{In}_2\text{O}_3$ .

DOI: 10.1103/PhysRevB.68.165104

PACS number(s): 71.20.Ps, 71.20.Nr, 78.70.En

## I. INTRODUCTION

The electronic structure of post-transition metal-oxide semiconductors (such as CdO,  $\text{In}_2\text{O}_3$ ,  $\text{SnO}_2$ , and Sn-doped  $\text{In}_2\text{O}_3$ ), has been a subject of enduring interest due to the potential use of such oxides as transparent electrical conductors.<sup>1–3</sup> One important feature of the electronic structure of transition-metal oxides is the hybridization between metal  $d$  orbitals and ligand oxygen  $p$  orbitals. Band structure theories indicate the strength of the hybridization that can occur in such systems, but observation of such hybridization has only been possible indirectly, via spectroscopies such as photoemission.<sup>4</sup> Soft x-ray emission spectroscopy (SXE) has recently been shown to be a technique that allows the *direct* measurement of the hybridization of metal  $d$  orbitals with ligand  $p$  orbitals.<sup>5,6</sup> In a SXE study of the valence band electronic structure of the  $\text{Al}_x\text{Ga}_{1-x}\text{N}$  alloy system, the hybridization of the shallow Ga  $3d$  core level with the N  $2p$  ligand states was clearly observed as a discrete emission feature of N  $2p$  character at the binding energy the Ga  $3d$  core level. In addition to allowing direct measurement of hybrid states, SXE also measures the bulk, elementally resolved, valence band partial density of states (PDOS).<sup>7–10</sup> The complementary technique of soft x-ray absorption (SXA) measures the elementally resolved PDOS for the unoccupied conduction band.<sup>11</sup>

Here we report a comprehensive SXE and SXA study of the valence and conduction band electronic structure of ZnO, CdO,  $\text{In}_2\text{O}_3$ ,  $\text{SnO}_2$  and Sn-doped  $\text{In}_2\text{O}_3$ . (Sn-doped  $\text{In}_2\text{O}_3$  is commonly referred to as ITO) For each oxide, we have measured the O  $2p$  valence and conduction band PDOS. We also directly observed shallow core-level hybridization in each of these oxides. The results of our measurements are compared to theory.

## II. EXPERIMENT

The experiments reported here were undertaken on soft x-ray undulator beamline X1B at the National Synchrotron Light Source (NSLS) at Brookhaven National Laboratory.<sup>12</sup> This beamline is equipped with a spherical grating monochromator. Soft x-ray emission spectra were recorded using a Nordgren-type grazing-incidence spherical grating spectrometer with a total energy resolution of  $\sim 0.4$  eV at the O  $K$  edge.<sup>9,13</sup> The resolution of the monochromator was set to 0.7 eV for SXE measurements, leading to a combined spectrometer/monochromator resolution of 0.85 eV for the resonant SXE spectra presented here. In order to obtain reasonable statistical accuracy in the SXE spectra the data was acquired for 60–90 min per spectrum. For soft x-ray absorption spectra, the resolution of the monochromator was set to 0.15 eV. SXA spectra were recorded both by the sample drain current technique to obtain the total electron yield and by measuring the total fluorescence yield with normal incidence of the incoming radiation. Both SXE and SXA experiments were performed with the samples at room temperature. Vacuum pressures during the measurements were below  $5.0 \times 10^{-9}$  Torr.

The CdO sample studied was a high purity (99.999%) polycrystalline pressed CdO pellet, previously used in a photoemission study.<sup>4</sup> The  $\text{In}_2\text{O}_3$ ,  $\text{SnO}_2$ , and ZnO samples were commercially available high purity (99.999%) powders and were mounted by either pressing the powder into clean indium foil or by pressing the powder onto a double-sided carbon conductive adhesive disc. The Sn-doped  $\text{In}_2\text{O}_3$  (ITO) sample studied was contained 10% Sn, and was a vacuum deposition grade sintered and fused homogeneous pellet.

## III. RESULTS AND DISCUSSION

An overview of the experiment is presented in Figs. 1, 2, and 3. Figure 1 shows a series of SXE and SXA spectra

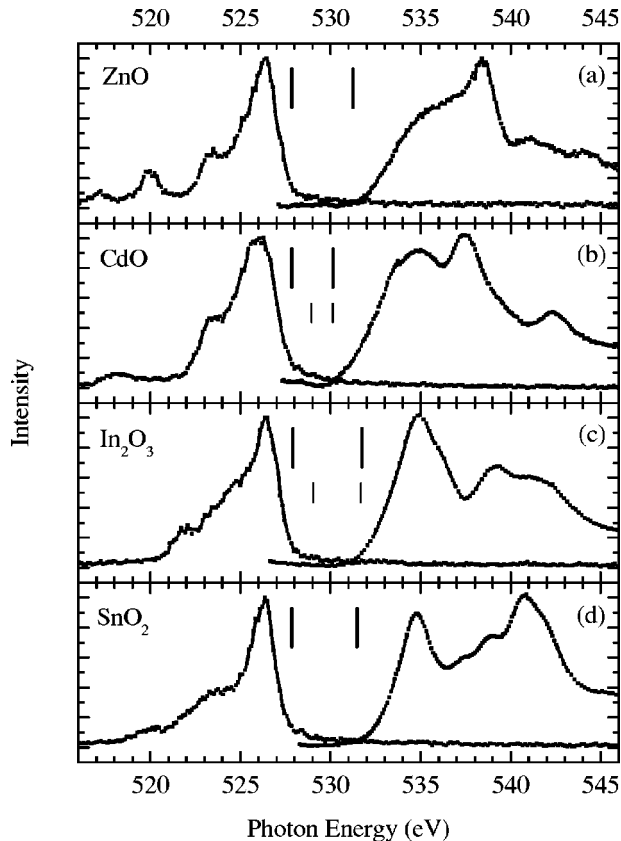


FIG. 1. O  $2p \rightarrow 1s$  SXE and O  $1s \rightarrow 2p$  SXA spectra for (a) ZnO, (b) CdO, (c)  $\text{In}_2\text{O}_3$ , and (d)  $\text{SnO}_2$ , respectively. The excitation energies were 566.6, 572.8, 566.6, and 562.3 eV respectively. The reported direct band gap for each oxide is indicated by long vertical bars, while the reported indirect gap is indicated by short vertical bars.

reflecting the elementally resolved O  $2p$  PDOS for the valence and conduction band states in ZnO, CdO,  $\text{In}_2\text{O}_3$ , and  $\text{SnO}_2$ . The SXE spectra were recorded with excitation photon energies well above the absorption threshold. Significant changes in the spectra can be observed through the series of oxides. Figure 2 presents the same set of SXE spectra as included in Fig. 1, but on expanded energy and intensity scales. As will be discussed, this allows emission due to shallow core level hybridization to be identified. Figure 3 presents a comparison of the SXE spectra for each oxide with published x-ray photoemission spectroscopy (XPS) results. The detailed results for each individual oxide are discussed below.

### A. ZnO

ZnO crystallizes in the wurtzite structure and has a band gap of 3.4 eV.<sup>14</sup> Many first principles calculations of ZnO have been published, focusing in particular on the electronic and structural properties.<sup>15–19</sup> It is clear from both the calculations and results of photoemission experiments that the zinc  $d$  electrons interact strongly with the oxygen  $p$  electrons.<sup>20,21</sup> More generally, Wei and Zunger theoretically examined the extent to which the metal  $d$  orbitals in IIB-VIA

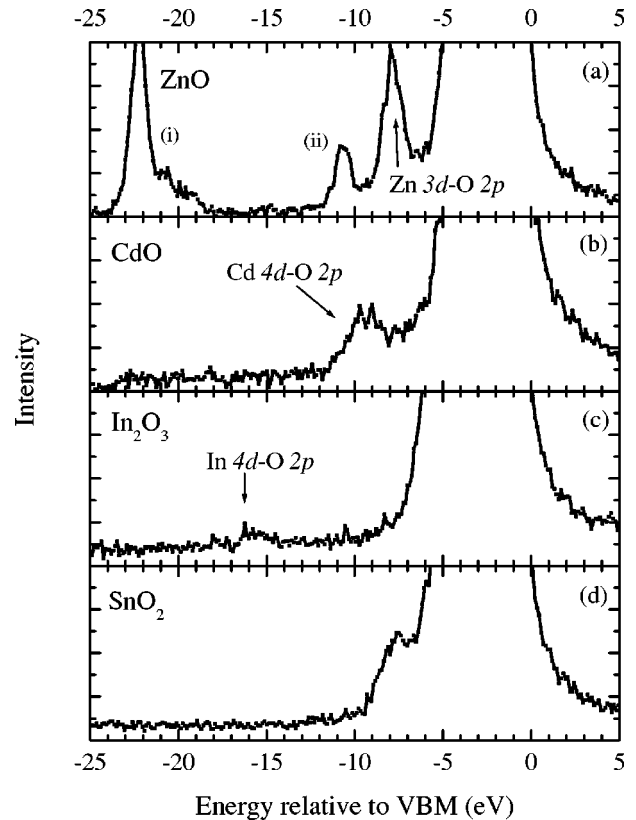


FIG. 2. The same SXE data as Fig. 1 plotted on an expanded energy scale. Metal  $d$ -ligand  $p$  hybridization peaks are indicated for (a) ZnO, (b) CdO, (c)  $\text{In}_2\text{O}_3$ , and (d)  $\text{SnO}_2$ . See the text for details, including explanation of features (i) and (ii) in (a).

semiconductors can be treated as corelike chemically inert states.<sup>22–24</sup> Relatively few theoretical investigations have explicitly accounted for this interaction, which is important for the determination of the energy of the Zn  $d$  states with respect to the highest (mostly O  $2p$ ) valence bands.<sup>17–19</sup>

Figure 1(a) shows the O  $1s$  SXE and SXA spectra for ZnO, reflecting the O  $2p$  resolved valence and conduction band states, and Fig. 2(a) shows the O  $2p \rightarrow 1s$  SXE over an extended range covering the binding energy of the Zn  $3d$  shallow core level. Figure 3(a) compares the O  $2p$  partial density of states (as measured here by SXE) to the total density of states (DOS) as measured by XPS.<sup>25</sup> The valence band maximum (VBM) in the SXE spectrum is estimated by a linear extrapolation of the leading edge of the valence band, while the energy scale of the XPS spectrum is as published.<sup>25</sup> (Note that a tail exists at the front of the valence band edge which is largely due to the effect of the core-hole lifetime Lorentzian broadening of the PDOS.) The XPS spectrum shows a strong feature at approximately 8 eV below the VBM due to photoemission from the Zn  $3d$  state. As is clear in Fig. 3(a), we observe an x-ray emission feature at the same energy. However, since this SXE spectrum is the result of creating a core hole on the O  $1s$  level, and the radiative decay is governed by strict dipole selection rules and is primarily intra-atomic,<sup>5,6</sup> we identify this feature at 8 eV below the VBM in the O  $2p \rightarrow 1s$  SXE spectrum as being due to emission resulting from the transition into O  $1s$  holes

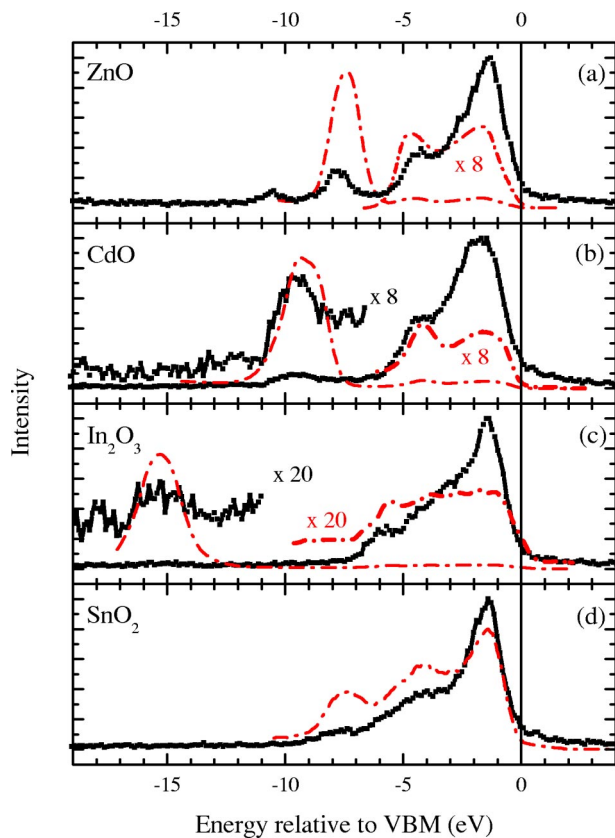


FIG. 3. O 2*p* PDOS as measured by SXE compared to valence band XPS measurements for (a) ZnO (Ref. 25), (b) CdO (Ref. 4), (c) In<sub>2</sub>O<sub>3</sub> (Ref. 38), and (d) SnO<sub>2</sub> (Ref. 47). The valence band regions of the XPS spectra are scaled (dash-dotted lines) for comparison with the SXE spectra. The spectra are all aligned to the valence band maxima of the respective materials.

of electrons in O 2*p* states hybridized with Zn 3*d* shallow core level states. While O 1*s* SXE is an unambiguous probe of the O 2*p* hybridization with the metal *d* states, the same is not true for metal ion SXE. SXE at the metal ion 2*p* (or 3*p*) edges will probe the metal *nd* hybridization with the O 2*p* states it is not unambiguous as it will also probe metal (*n* + 1)*s* hybridization with the metal *nd* states. (Note that the emission features observed at approximately (i) 11 eV and (ii) 22 eV below the VBM that are visible in Fig. 2(a) are due to Zn *L*<sub>2,3</sub> emission resulting from the excitation of Zn 2*p* holes with second order light from the monochromator).

Figure 4 compares our measured valence and conduction band PDOS for ZnO with the results of a published tight binding calculation which treats the Zn 3*d* electron self-consistently with the rest of the valence electrons,<sup>19</sup> and with a local density approximation calculation.<sup>18</sup> The calculated O 2*p* PDOS agree reasonably well with the measured valence band PDOS near the VBM. However, neither calculation agrees with the energy or intensity of the measured emission from the hybridized Zn 3*d*–O 2*p* states. The Zn 3*d*–O 2*p* soft x-ray emission feature is observed at an energy of 8 eV below the VBM unlike the calculation of Yang and Dy which predicts these states to be located at an energy of approximately 9.5 eV. However, their estimate of the relative inten-

sity of the feature agrees well with our observation. In the calculation by Xu and Ching, as well as that of Schröer *et al.*, the *p*–*d* interaction strength is overestimated, locating the Zn 3*d* bands from 6.5 to 4 eV below the VBM, with a consequent overestimation of the intensity of the hybridization feature in the O 2*p* PDOS.<sup>17,18</sup> A modified local density approximation approach that includes self-interaction correction has been proposed by Vogel *et al.* and results in better agreement in terms of the bandwidth of the O 2*p* states, the band gap and the location of the Zn 3*d* band below the VBM; no calculation of the PDOS was presented.<sup>26,27</sup> The SXE and XPS results for ZnO presented in Fig. 3(a) agree reasonably well with each other in the valence band region, with the caveat that SXE measures the elementally resolved O 2*p* PDOS, while XPS measures the nonelementally resolved valence band DOS. The ratio of intensities of the two peaks in the valence band SXE and XPS spectra differ, which is due to the fact that lower energy state has a large component of Zn 4*s* character in the measured DOS. In general for these oxides, the O 2*p* valence band feature observed at higher emission energy is that of oxygen 2*p* bands of nonbonding character, while the lower emission energy peak is those bands formed from oxygen 2*p* bonding orbitals mixing with the metal *s* states. There is little dependence of the observed SXE spectrum with increasing incident excitation energy other than the leading edge of the valence band becoming less well. This is due to multihole emission resulting from the simultaneous creation of an O 2*s* hole.

There is less uniform agreement between the published calculations for the O 2*p* conduction band PDOS and our SXA measurements than we found between our valence band SXE measurements and the same calculations. In particular, the calculations of Yang and Dy predict a gap in the conduction band PDOS between 7.5 and 10 eV above the VBM. This is in contrast with both the observed SXA spectrum representing the O 2*p* conduction band PDOS [Fig. 1(a)] and also the calculations of Schröer and Xu which both show a continuous density of states.<sup>17,18</sup>

## B. CdO

CdO is unusual among the IIB–VI binary compound semiconductors as it exists solely in a face-centered-cubic rock-salt structure which is more typical of the ionic insulators. All other Cd and Zn oxides and chalcogenides crystallize in either the cubic zinc-blende or the hexagonal wurtzite structure in which the metal is tetrahedrally coordinated. In CdO the metal cation is octahedrally coordinated. The band structure of CdO has been calculated on numerous occasions.<sup>4,16</sup> Wei and Zunger, in an examination of IIB–VIA semiconductors, used calculational techniques that treat the *d* electrons on the same footing as the other valence electrons, and found significant *d*-electron effects on band gaps and also on ground-state properties such as equilibrium lattice parameters and cohesive energies.<sup>22–24</sup> Likewise, the interaction between the valence O 2*p* states and the Cd 4*d* core states is predicted to play a large role in determining the type of band gap.<sup>16</sup> Jaffe *et al.* noted that a hallmark of these band structures is that the VBM is not at the center of the Brillouin

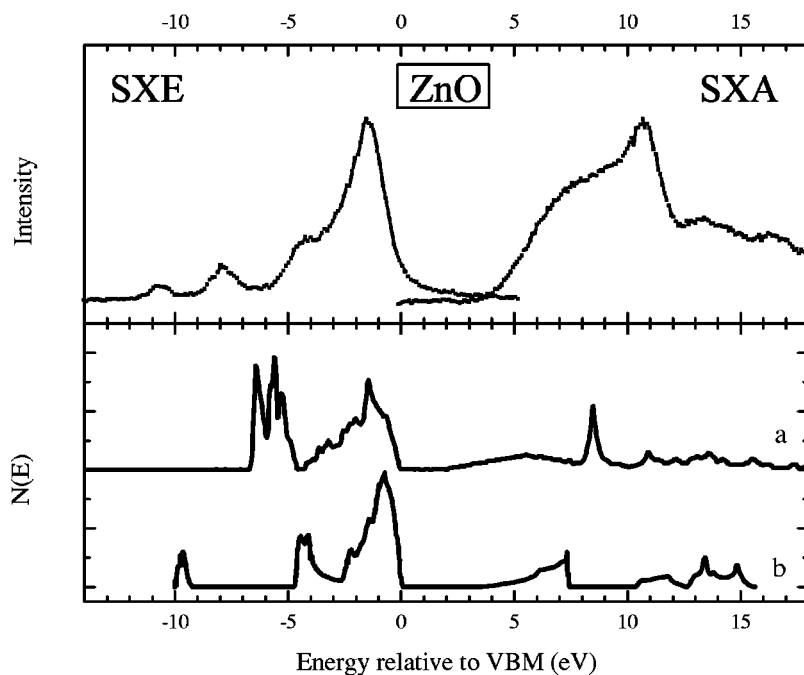


FIG. 4. ZnO O 2p PDOS measured by SXE and SXA (upper graph), compared to two valence band O 2p PDOS calculations (lower graph). The upper calculation (a) is that of Xu and Ching (Ref. 18) while the lower (b) is that of Yang and Dy (Ref. 19). The feature seen in emission at an energy of approximately 10.8 eV is second order Zn  $L_{2,3}$  emission due to excitation from second order light in the monochromator.

zone (leading to an indirect band gap), in contrast to the situation in tetrahedrally coordinated II-VI semiconductors.<sup>16</sup> The indirect gap is predicted to be a direct consequence of the hybridization of O 2p derived orbitals with Cd 4d states, combined with octahedral point symmetry.<sup>16</sup> The magnitude of this interaction is generally gauged by the energy separation between the top of the O 2p valence band and the Cd 4d shallow core states.

The detailed band structure and densities of states for CdO were recently calculated using both periodic Hartree-Fock and density functional methods by Dou *et al.*<sup>4</sup> In this calculation the single-particle orbitals of the periodic system were expanded as a linear combination of atomic orbitals. The exchange and correlation potentials were treated using both the exact exchange interaction (periodic Hartree-Fock theory) and density functional theory in the local density approximation. The results of these calculations were compared to XPS spectra measured in the region of the O 2p valence band and the Cd 4d shallow core level. The XPS spectra allow the energy separation between the top of the O 2p valence band and Cd 4d shallow core states to be obtained. By consideration of the photon energy dependence of the spectral features (i.e., their photoelectric cross-section), indirect evidence of O 2p–Cd 4d mixing was deduced.<sup>4</sup> Our SXE spectra presented in Figs. 2(b) and 3(b) clearly show direct evidence of the existence of this hybridization. We compare our SXE measurement of the O 2p PDOS with the XPS measurements of Dou *et al.* in Fig. 3(b).<sup>4</sup> There is good agreement between the SXE measurement of the O 2p PDOS and the XPS measurements of the DOS for the position of the Cd 4d core-level XPS peak, the Cd 4d hybridization peak, and the features of the valence band. Similarly to the case in ZnO the lower peak in the valence band at about 4 eV below the VBM has significant contribution from Cd 5s states.

Comparing the results of the Hartree-Fock calculation of the O 2p valence band PDOS with the SXE spectra obtained here (Fig. 5) it can be seen that there is a good overall agreement between the experiment and theory.<sup>4</sup> The observed width of the valence band appears to be slightly greater than 5 eV but is in accord with the calculation once instrumental and lifetime broadening are taken into account. The separation between the hybridized Cd 4d–O 2p emission peak and the O 2p valence band is observed to be smaller than that predicted by the Hartree-Fock calculation which nevertheless gives a better estimate than the density functional calculation of the same authors.<sup>4</sup> The only significant discrepancy between the calculated and observed valence band PDOS is in the relative intensity of the two peaks in the O 2p valence band, where the intensity of the high binding energy peak appears to be overestimated. The CdO O 2p SXE spectra display small changes as the excitation energy is varied. At excitation energies between 534 and 542 eV, the shoulder observed at lower emission energy in the SXE spectrum becomes more pronounced, and for excitation energies above 560 eV the emission intensity close to the leading edge of the valence band increases due to multihole effects. None of the previous calculations of the band structure of CdO have presented the PDOS of the conduction band, and so we cannot compare these results directly to our measured SXA spectrum. The conduction band consists primarily of Cd 5s states with some admixture of O 2s.

The magnitude of the band gap in CdO is an issue of some controversy. The lowest energy indirect band gap of CdO is usually quoted to be 0.55 eV at room temperature and 0.84 eV at 100 K, while the direct band gap is 2.28 eV.<sup>28</sup> However, previous photoemission experiments indicate that the gap at room temperature must be more than 1 eV.<sup>29,30</sup> This assertion is based on the observation that the O 2p valence band onset in photoemission from oxygen deficient



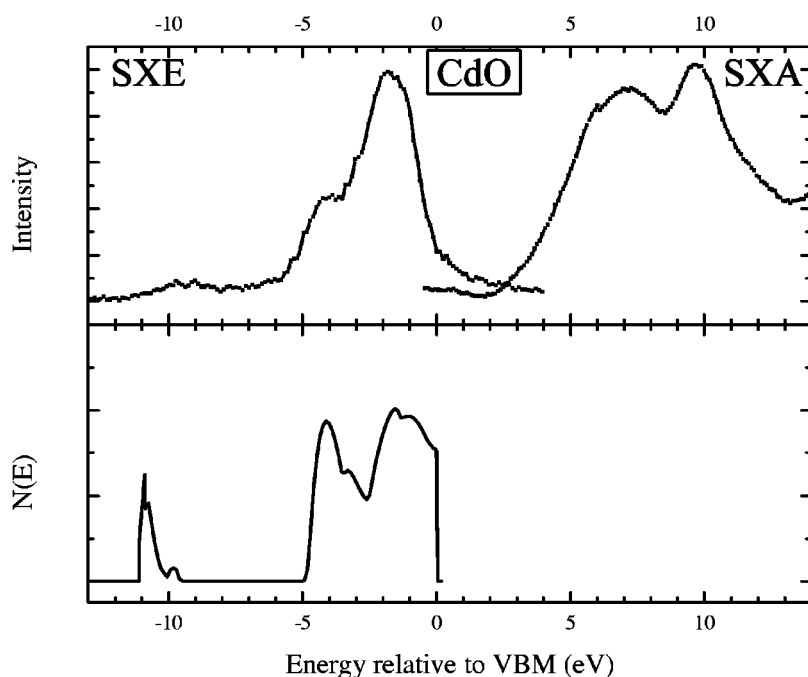


FIG. 5. CdO O 2p PDOS measured by SXE and SXA (upper graph) compared to the calculated valence band O 2s/2p PDOS of Dou *et al.* (Ref. 4).

(vacuum annealed) CdO is, at 1.53 eV, relative to the Fermi-Dirac-like onset associated with electrons in the conduction band. These electrons in the conduction band arise from oxygen vacancies in the vacuum annealed CdO, and have a carrier concentration of approximately  $0.85 \times 10^{20} \text{ cm}^{-3}$ .<sup>29,30</sup> This implies that the conduction electron gas is highly degenerate. Taking account of the variation of the effective mass with the carrier concentration, the Fermi energy is estimated to lie 0.54 eV above the conduction band minimum. Thus the energy separation between the bottom of the conduction band and the top of the valence band is 0.99 eV in defective CdO. This value must in turn be slightly lower than the corresponding gap in stoichiometric CdO because of the band gap shrinkage or renormalization that arises from degenerate *n*-type doping. Following Hamberg *et al.*<sup>31</sup> and Sanon *et al.*<sup>32</sup> we estimate this shrinkage to be  $0.20 \pm 0.05$  eV at a carrier concentration of  $10^{20} \text{ cm}^{-3}$ . This reevaluation of the photoemission measurements leads to a revised estimate of about 1.2 eV for the indirect gap of undoped CdO at room temperature. This value of 1.2 eV is displayed in Fig. 1(b) for the indirect gap. However, the SXE and SXA spectra for the occupied and unoccupied O 2p states in CdO presented in Fig. 5 reveal a much larger elementally specific band gap of almost 2 eV. The exact magnitude of the gap is difficult to determine due to the extended leading edge on the absorption spectrum, but it is clear that our measurements indicate a gap significantly larger than 0.55 eV.

### C. $\text{In}_2\text{O}_3$

Indium oxide crystallizes in the bixbyite crystal structure and is a wide band gap semiconductor with a direct gap of 3.75 eV and an indirect gap of 2.6 eV.<sup>33</sup> Relatively few band structure or tight binding calculations have been reported for indium oxide, due in part to the 40-atom unit cell.<sup>34,35</sup> Al-

banesi *et al.* carried out an empirical tight-binding calculation as part of a systematic analysis of crystalline InP oxides, but without including the In 4d as part of the basis set.<sup>36</sup> Subsequent calculations were performed from first principles using the discrete variational  $X\alpha$  method on model clusters of indium oxide by Tanaka *et al.*<sup>34</sup> Odaka *et al.* carried out a first principles calculation based on density functional theory using the characteristics of the linear muffin-tin orbital method with the atomic sphere approximation.<sup>35</sup> More recently Mi *et al.* performed a first principles pseudopotential calculation within the density functional formalism in order to study the band structure of indium oxide, tin oxide, and zinc oxide.<sup>15</sup> While Mi *et al.* obtained the best agreement between calculated band gaps and experimental results, all the theoretical results showed close agreement in comparison to available valence band XPS data.

Odaka *et al.* predicted a strong hybridization between the In 4d orbitals and the O 2p orbitals, not only at the binding energy of the 4d electron, but also throughout the O 2p valence band.<sup>35</sup> Their theoretical results for the DOS agreed well with the experimental XPS and bremsstrahlung isochromat spectroscopy spectra.<sup>37</sup> Tanaka *et al.* also predicted a hybridization of the filled In 4d orbital with the O 2s and 2p orbitals and the contribution of the In 4d bands to the O 2p states in the valence band.<sup>34</sup> It was further noted that the observed XPS spectra of the valence band strongly reflects the structure of the In 4d PDOS due to the much higher In 4d partial photoionization cross section in comparison to that of O 2p.<sup>34,38</sup> However, there is a discrepancy between the XPS results of Orita *et al.* and those of Barr and Liu, which indicates the binding energies of the shallow core In 4d electrons to be 14 and 18 eV, respectively.<sup>37,38</sup>

Figure 1(c) presents the O 2p SXE and SXA spectra obtained from  $\text{In}_2\text{O}_3$ , while Fig. 2(c) presents the SXE spectrum over an expanded energy and intensity range. The In

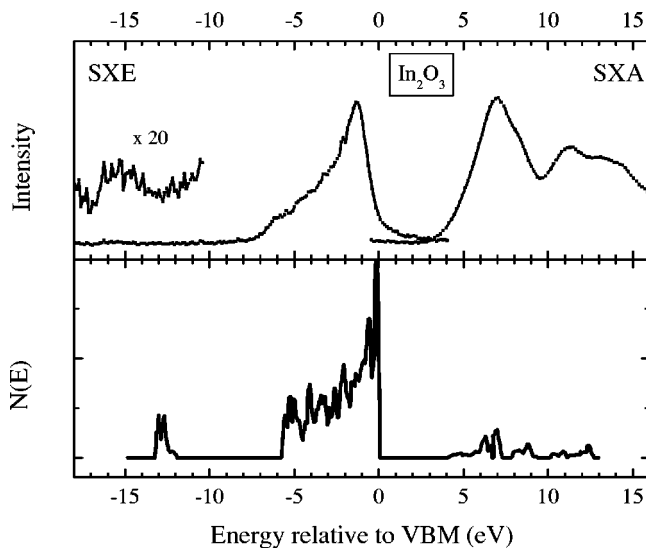


FIG. 6.  $\text{In}_2\text{O}_3$  O  $2p$  PDOS measured by SXE and SXA (upper graph) compared to the O  $2p$  PDOS calculation of Odaka *et al.* (Ref. 35).

$4d$ -O  $2p$  hybridization feature can be easily identified at an energy of 15–16 eV below the VBM. This is consistent with the binding energy of the In  $4d$  states of 18 eV obtained by Barr and Liu; Fig. 3(c) compares their XPS data with our SXE spectrum, where we have shifted their energy scale to align the observed In  $4d$  shallow core levels.<sup>38</sup> With this shift, the valence bands from the two measurements also align. Figure 6 shows both the  $\text{In}_2\text{O}_3$  O  $2p$  SXA spectrum and the (above threshold) SXE spectrum, and compares them to the calculated O  $2p$  PDOS of Odaka *et al.*<sup>35</sup> The O  $2p$  states in the valence band have a larger bandwidth ( $\sim 7$  eV) than that predicted by the cluster calculations ( $\sim 5$  eV) but a similar overall distribution to that measured by SXE. The predicted location of the In  $4d$  bands is  $\sim 3$  eV lower in binding energy than the SXE spectrum indicates. The conduction band O  $2p$  PDOS is also similar to the SXA spectrum measured here, with the first peak corresponding to a mixture of O  $2p$  and In  $5s$  states, and the subsequent features above 536 eV being due to mixtures of O  $2p$  and In  $5p$  states. Little excitation energy dependence of the SXE spectra was observed.

#### D. $\text{SnO}_2$

Tin oxide,  $\text{SnO}_2$ , the last binary oxide compound in our study, exists in a rutile crystal structure,<sup>39</sup> and was initially reported to have a band gap of 3.8 eV.<sup>40</sup> However, it has been pointed out that a significant variation of this value exists in the literature ranging between 4.3 and 2.25 eV,<sup>41</sup> and a two-photon measurement of the dipole-forbidden gap yielded a value of 3.62 eV.<sup>42</sup> Numerous band structure calculations for both the bulk electronic structure and the surface electronic structure of  $\text{SnO}_2$  are available in the literature.<sup>39,43–45</sup> These have employed variational transition state  $X_\alpha$ , linear muffin-tin orbital (LMTO), and tight-binding methods. Likewise, there have been many XPS studies of  $\text{SnO}_2$ .<sup>43,46–49</sup>

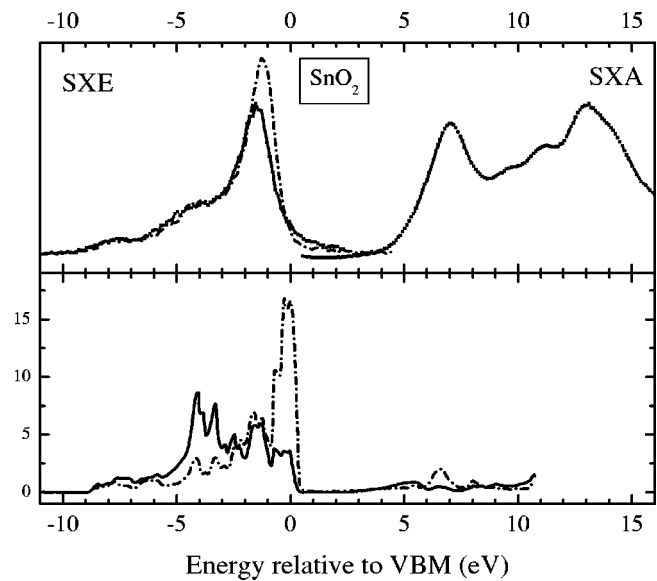


FIG. 7.  $\text{SnO}_2$  O  $2p$  PDOS measured by SXE and SXA (upper graph) compared with the LMTO calculations of Medvedeva *et al.* (Ref. 44). Two SXE spectra are shown: (a)  $h\nu = 550.4$  eV (solid line), above the absorption threshold, and (b)  $h\nu = 534.7$  eV (dash-dotted line), at the first absorption peak. The SXA spectrum (solid line) is also shown. In the lower panel, the O  $2p$  unbroadened PDOS for the two oxygen sites in the  $\text{SnO}_2$  rutile crystal structure are shown as  $\text{O}_1$  (solid line) and  $\text{O}_2$  (dash-dotted line). See the text for details.

The O  $2p$  SXE and SXA spectra of  $\text{SnO}_2$  are presented in Fig. 1(d), and the O  $2p$  SXE spectrum is compared with the measured valence band XPS spectrum of Kover *et al.* in Fig. 3(d).<sup>47</sup> This XPS spectrum is in good agreement with those of Egdel and Themlin; the higher resolution spectra of Egdel exhibit a shoulder on the low binding-energy side that tails into the bulk band gap due to reduction of half the surface Sn atoms from Sn(IV) to Sn(II) and is not shown here.<sup>46,48,49</sup> This high resolution study gives the positions of the three prominent features as being at binding energies of 4.95, 7.46, and 11.07 eV with respect to the Fermi energy (the valence band offset being 3.60 eV) which agrees well with our observed SXE spectrum and is used to align the spectrum of Kover *et al.* The calculated bulk DOS indicates that the first peak is O  $2p$  in character, the second being a mixture of Sn  $5p$  and O  $2p$  and that the highest binding energy peak exists as a mixture of Sn  $5s$  and O  $2p$  states.<sup>46</sup> The strong first peak has been previously assigned to non-bonding O  $2p$  orbitals oriented perpendicular to the Sn-O axis and which contribute little to the chemical bonding, in agreement with the more recent calculations of Medvedeva *et al.*<sup>44</sup> It should be noted that the binding energy for the Sn  $4d$  orbital is 26.28 eV below the Fermi energy in undoped  $\text{SnO}_2$ , and unlike the other oxides studied here, no discernible metal-O  $2p$  hybridization peak could be observed in the SXE spectrum (i.e., in the region 22–23 eV below the VBM).<sup>46</sup>

Figure 7 compares the measured O  $2p$  PDOS to the calculated O  $2p$  PDOS of Medvedeva *et al.*, where the non-equivalency of the oxygen atomic orbitals in rutile-type

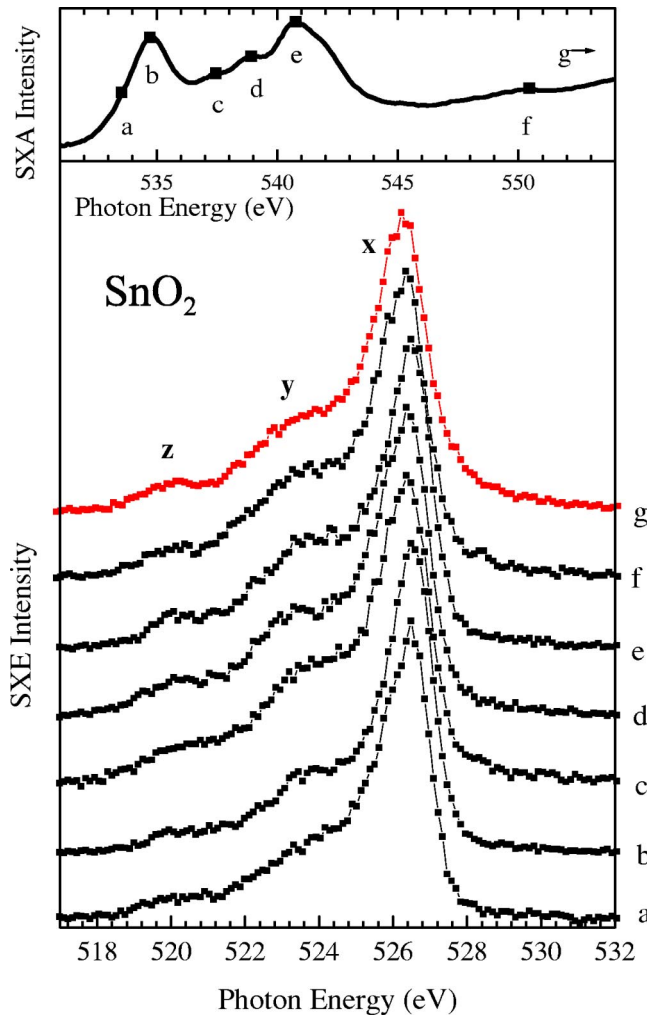


FIG. 8. SXE spectra from  $\text{SnO}_2$  as a function of excitation energy (main panel). Also shown is the SXA spectrum of  $\text{SnO}_2$  (upper panel). The excitation energy of the recorded SXE spectra, each denoted by a letter, is indicated by markers and the corresponding letter at that point on the SXA spectrum. The uppermost SXE spectrum is obtained at an energy of 562.3 eV approximately 30 eV above the threshold. The three main emission features are labeled  $x$ ,  $y$ , and  $z$ .

structure is taken into account.<sup>44</sup> Thus the O  $2p$  PDOS of states is shown for two sets of oxygen orbitals; the  $\text{O}_1$  set of paired orbitals is where the oxygen orbitals are in the plane of the  $\text{Sn}_3\text{O}$  trigonal configuration while the  $\text{O}_2$  set are the single orbitals perpendicular to the bonding plane. The calculation indicates that the low binding energy region of the O  $2p$  valence band consists of states of single oxygen orbitals, while the bottom of the valence band consists of mixed Sn  $5s$  and O  $2p$  states (mainly of the  $\text{O}_1$  set). It can be seen that in the conduction band region there is a point about 6.5 eV above the VBM where the PDOS is dominated by states at the  $\text{O}_2$  states, while at most other points the weighting is more equal. Thus, in addition to the above threshold SXE spectrum we also show an on-resonance SXE spectrum of  $\text{SnO}_2$  which will be explained in detail. Figure 8 shows the SXA spectrum obtained from  $\text{SnO}_2$  at the top of the figure

with a succession of resonantly excited O  $2p$  SXE spectra where the excitation energy used to obtain each SXE spectrum is marked and indicated on the SXA spectrum. The point where the  $\text{O}_2$  states dominate the conduction band PDOS corresponds to the SXE spectrum labeled as  $b$ , and it is this spectrum that is also shown in Fig. 7.

In the O  $2p$  SXA spectrum of  $\text{SnO}_2$  shown at the top of Fig. 8, transitions to the unoccupied states in the conduction band may be clearly identified by comparison to a simple molecular-orbital picture.<sup>50</sup> In  $\text{SnO}_2$ , a rutile structure, the space group is  $D_{4h}$ ,<sup>14</sup> while in a molecular-orbital picture the symmetry of the  $\text{SnO}_6$  polyhedra may be considered to be  $D_{2h}$ . Thus the first band at 534.73 eV corresponds to transitions to the  $a_g$  state (O  $2p$  and Sn  $5s$ ) and the three successive bands can be identified as transitions to the  $b_{1u}$ ,  $b_{2u}$ , and  $b_{3u}$  states (O  $2p$  and Sn  $5p$ ) at energies of 537.35, 538.75, and 540.62 eV. Using the same molecular-orbital picture, the three peaks observed in the valence band (labeled  $x$ ,  $y$ , and  $z$ ) can be ascribed to the  $2a_g$ ,  $b_{1u} + b_{2u} + b_{3u}$ , and  $a_g$  states, respectively.

SXE spectra were recorded at the incident photon energies indicated on the SXA spectrum shown in Fig. 8. The SXE spectra taken at points  $a$  and  $b$ , immediately before and coincident with the  $a_g$  state in the conduction band (an incident photon energy of 534.7 eV), can be contrasted with spectrum  $c$ . In spectrum  $b$  the intensity of the emission peak nearest the VBM (labeled  $x$ ) is greatly enhanced and the centroid shifted to higher energy by about 0.25 eV compared to spectrum  $c$ . In later spectra ( $c$  and above) the ratios of the intensities of the three peaks ( $x:y:z$ ) are approximately that obtained in spectrum  $g$  with the incident photon energy at 562.3 eV. The peak of the emission in spectra  $c$  and  $d$  is coincident in energy with the above threshold PDOS (spectrum  $g$ ). Going from spectrum  $d$  to spectrum  $e$  with an incident energy at 540.9 eV, the emission feature  $x$  shifts to 0.1-eV higher energy at the peak and about 0.2 eV on the high binding energy side. This shift is then restored at higher excitation energies such as in spectra  $f$  and  $g$ . As indicated above this behavior can be explained as a PDOS state effect in the SXE spectrum through the LMTO band structure calculations of Medvedeva *et al.*<sup>44</sup> Thus at excitation points  $a$  and  $b$ , the O  $1s$  hole that is created is predominantly due to absorption to  $\text{O}_2$  states with the resultant SXE spectrum reflecting the O  $2p$  PDOS of the  $\text{O}_2$  state. Hence in Fig. 7 we compare the calculated orbital-specific O  $2p$  PDOS with both the above threshold SXE spectrum and the SXE spectrum obtained at  $b$  (534.7 eV), where the latter reflects more closely the  $\text{O}_2$  PDOS while the former is a combination of the two.

### E. ITO (Sn-doped $\text{In}_2\text{O}_3$ )

In addition to the four binary post-transition-metal oxide compounds studied above we also report SXE and SXA spectra of Sn-doped- $\text{In}_2\text{O}_3$ , commonly known as ITO, indium tin oxide. ITO is the transparent conductor of choice for the electronics industry and is used in a variety of applications from coatings that prevent frosting of supermarket freezer doors to contact layers in flat panel liquid crystal



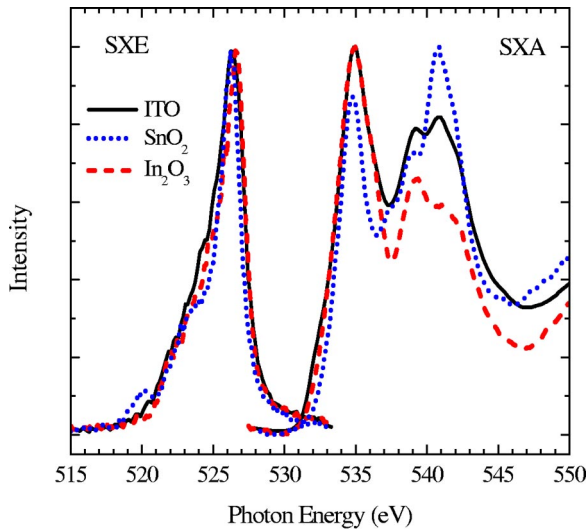


FIG. 9. Comparison of measured SXA and SXE of ITO, 10% Sn-doped  $\text{In}_2\text{O}_3$ , with those of  $\text{SnO}_2$  and  $\text{In}_2\text{O}_3$ . The SXE spectra for the  $\text{SnO}_2$  and  $\text{In}_2\text{O}_3$  are those shown in Fig. 1. The excitation energy for the ITO spectrum was 540.8 eV.

display-thin film transistor (LCD-TFT) displays. In ITO, the Sn is a substitutional dopant for In in the  $\text{In}_2\text{O}_3$  bixbyite structure and for typical commercial uses the percentage substitution approaches 10% depending upon the application. Numerous studies of the resistivity and optical properties of ITO thin films have been undertaken with a view to optimizing the desirable properties for the commercial market.<sup>31,51</sup> Although there have been calculations of the band structure of ITO, these have primarily addressed the issue of optical and transport properties.<sup>52</sup> Recently there have been some calculations which have addressed the basic electronic properties directly.<sup>53,54</sup> These have been the first *ab initio* studies of ITO since the original schematic energy band model of Fan and Goodenough was proposed on the basis of their XPS measurements.<sup>55</sup> The density functional calculations of Odaka *et al.* proceed from their earlier calculations of  $\text{In}_2\text{O}_3$  while those of Mryasov and Freeman are local-density full potential linear muffin-tin orbital calculations.<sup>35,53,54</sup>

We recorded SXE and SXA spectra from both a vacuum deposition grade sintered ITO pellet and from a commercially available ITO thin film sample. These results are compared to those of  $\text{In}_2\text{O}_3$  and  $\text{SnO}_2$ . Figure 9 shows the SXA and SXE spectra obtained from a 10% doped ITO sample in comparison with the SXA and SXE spectra of  $\text{In}_2\text{O}_3$  and  $\text{SnO}_2$ . The presence of Sn in the  $\text{In}_2\text{O}_3$  structure modifies the SXA spectrum from that of  $\text{In}_2\text{O}_3$ , particularly in the energy region around 541 eV. The SXE spectrum shows smaller changes, mainly in the width of the main emission feature which is broadened slightly compared to that of  $\text{In}_2\text{O}_3$ , with an indication of a small feature developing at the bottom of the valence band. No significant change is observed in either the position or strength of the  $\text{In } 4d\text{--O } 2p$  hybridization feature from that of pure  $\text{In}_2\text{O}_3$ , nor is any deviation from the behavior of the SXE spectrum observed as the excitation energy is swept through from the O  $1s$  threshold. Examining the conduction band edge, there is a small increase in weight

in the region of 532 eV and comparing with both the calculations gives an indication that this is due to a Sn  $5s$  state contributing to the conduction band.<sup>53,54</sup>

The carrier concentration in commercial ITO is typically around  $7 \times 10^{20} \text{ cm}^{-3}$ , and the Fermi level lies about 0.85 eV above the conduction band minimum.<sup>56</sup> In a rigid band model one might therefore expect a Moss-Burnstein type shift in the SXA onset to higher energy by this amount. However the rigid band shift will be offset by an expected band gap renormalization of approximately 0.36 eV.<sup>31</sup> The situation is further complicated by the fact that the core hole in the SXA experiment induces a screening response from the conduction electron gas.<sup>46,56,57</sup> This splits the spectral weight of the core hole into screened and unscreened components, with the separation between the two being determined by the plasmon energy of the conduction electron gas. This energy is of the order of 0.7 eV for typical commercial ITO samples. The presence of a O  $1s$  core hole plasmon satellite structure may be responsible for observation of a distinct shoulder at about 532 eV in the SXA onset of the ITO sample, although hybridization of O  $2p$  states with Sn  $5s$  states may also lead to the same observation.

#### IV. CONCLUSION

In the sequence  $\text{CdO} \rightarrow \text{In}_2\text{O}_3 \rightarrow \text{SnO}_2$ , both the binding energy of the metal  $4d$  shallow core level (Fig. 2) and the elementally specific O band gap (Fig. 1) increase with the increasing atomic number of the metal atom. Thus as the binding energy increases the metal  $4d\text{--oxygen } 2p$  interaction decreases. Figure 2 clearly shows that the position of the hybridization peak in the SXE spectrum progresses to higher binding energies through this sequence while simultaneously the intensity of the hybridization emission feature decreases rapidly. In fact, in the case of  $\text{SnO}_2$ , the hybridization emission peak is not detectable through SXE though from a comparison with XPS measurements the binding energy of the Sn  $4d$  level is at 22–23 eV below the VBM. Previously the only evidence available of Cd  $4d\text{--O } 2p$  mixing in CdO was indirectly observed through enhancements in the intensities of constant initial state XPS spectra observed in the region of a maximum in the Cd  $4d$  cross section profile.<sup>4</sup> Soft x-ray emission spectroscopy provides direct evidence of this hybridization. Further, a reinterpretation of photoemission results from CdO yields an estimated band gap of 1.2 eV, much larger than the accepted value for the indirect band gap of 0.55 eV.<sup>29,30</sup> This increased value for the band gap is supported by the current measurement of the elementally resolved O  $2p$  PDOS by SXE and SXA. In all cases the separation between the measured hybridization peak and the valence band maximum coincides with the binding energies of the metal  $d$  electrons measured by XPS. A comparison is also made between the observed local partial density of states of both the conduction and valence bands with available calculations. It was noted by Vogel *et al.*, specifically with regard to calculations of the band structure of ZnO, that the downward move of the metal  $d$  bands and the weakened  $p\text{--}d$  hybridization on going from local density approximation (LDA) calculations to a self-interaction-corrected LDA result



in both an opening of the gap and an increase in the bandwidth of the O 2*p* valence band.<sup>26,27</sup> Figure 2 clearly shows an increase in the bandwidth of the valence band as the metal *d* bands shift to higher binding energy, although it is to be expected that there is also an increasing contribution of metal 5*s* states to the valence band. As can be seen from Fig. 1, there is a striking similarity in the conduction band edges of all these materials. In each case the bottom of the conduction band is dominated by a highly dispersive band composed of metal 4*s* (Zn) or metal 5*s* states hybridized with O 2*p* states. This dispersive band leads to the distinctive conduction band edges seen here and Mryasov and Freeman have stated that this also leads to the observed high Burstein-Moss shifts in these materials, that is, shifts of the optical absorption edge with sufficient doping.<sup>31,51</sup> Finally, rocksalt CdO, bixbyite In<sub>2</sub>O<sub>3</sub>, and rutile SnO<sub>2</sub> all adopt structures with metal cat-

ions in sites with locally centrosymmetric coordination. This prevents hybridization of O 2*p* states with metal 4*d* states at the zone center, but mixing away from zone center leads to indirect band gaps for CdO and In<sub>2</sub>O<sub>3</sub>.

### ACKNOWLEDGMENTS

The Boston University program is supported in part by the Department of Energy under Contract No. DE-FG02-98ER45680. The x-ray emission spectrometer is funded by the U.S. Army Research Office under Grant No. DAAH04-95-0014. The experiments at the NSLS are supported by the U.S. Department of Energy, Division of Materials and Chemical Sciences. P.J.R. acknowledges the support of the William V. Shannon Memorial Fellowship. The authors thank Eileen Nugent for assistance with experiments.

<sup>†</sup>Present address: Advanced Photon Source, Argonne National Laboratory.

\*Author to whom correspondence should be addressed. Electronic address: ksmith@bu.edu

<sup>1</sup>A. J. Freeman, K. R. Poeppelmeier, T. O. Mason, R. P. H. Chang, and T. J. Marks, MRS Bull. **25**, 45 (2000).

<sup>2</sup>T. J. Coutts, D. L. Young, X. Li, W. P. Mulligan, and X. Wu, J. Vac. Sci. Technol. A **18**, 2646 (2000).

<sup>3</sup>X. Wu, T. J. Coutts, and W. P. Mulligan, J. Vac. Sci. Technol. A **15**, 1057 (1997).

<sup>4</sup>Y. Dou, R. G. Egdell, D. S. L. Law, N. M. Harrison, and B. G. Searle, J. Phys.: Condens. Matter **10**, 8447 (1998).

<sup>5</sup>L.-C. Duda, C. B. Stagarescu, J. Downes, K. E. Smith, D. Korakakis, T. D. Moustakas, J. Guo, and J. Nordgren, Phys. Rev. B **58**, 1928 (1998).

<sup>6</sup>C. B. Stagarescu, L.-C. Duda, K. E. Smith, J. H. Guo, J. Nordgren, R. Singh, and T. D. Moustakas, Phys. Rev. B **54**, 17 335 (1996).

<sup>7</sup>T. A. Callcott, C. H. Zhang, D. L. Ederer, D. R. Mueller, J. E. Rubensson, and E. T. Arakawa, Nucl. Instrum. Methods Phys. Res. A **291**, 13 (1990).

<sup>8</sup>J. A. Carlisle, S. R. Blankenship, R. N. Smith, E. L. Shirley, L. J. Terminello, J. J. Jia, T. A. Callcott, and D. L. Ederer, J. Electron Spectrosc. Relat. Phenom. **103**, 839 (1999).

<sup>9</sup>J. Nordgren, G. Bray, S. Cramm, R. Nyholm, J. E. Rubensson, and N. Wassdahl, Rev. Sci. Instrum. **60**, 1690 (1989).

<sup>10</sup>L. G. Paratt, Rev. Mod. Phys. **31**, 616 (1959).

<sup>11</sup>J. Stöhr, *NEXAFS Spectroscopy* (Springer, Berlin, 1992).

<sup>12</sup>K. J. Randall, W. Eberhardt, J. Feldhaus, W. Erlebach, A. M. Bradshaw, Z. Xu, P. D. Johnson, and Y. Ma, Nucl. Instrum. Methods Phys. Res. A **319**, 101 (1992).

<sup>13</sup>J. Nordgren and R. Nyholm, Nucl. Instrum. Methods Phys. Res. A **246**, 242 (1986).

<sup>14</sup>R. Matz and H. Lueth, Appl. Phys. (Berlin) **18**, 123 (1979).

<sup>15</sup>Y. M. Mi, H. Odaka, and S. Iwata, Jpn. J. Appl. Phys. **38**, 3453 (1999).

<sup>16</sup>J. E. Jaffe, R. Pandey, and A. B. Kunz, Phys. Rev. B **43**, 14 030 (1991).

<sup>17</sup>P. Schroer, P. Kruger, and J. Pollmann, Phys. Rev. B **47**, 6971 (1993).

<sup>18</sup>Y. N. Xu and W. Y. Ching, Phys. Rev. B **48**, 4335 (1993).

<sup>19</sup>C. K. Yang and K. S. Dy, Solid State Commun. **88**, 491 (1993).

<sup>20</sup>I. Ivanov and J. Pollmann, Phys. Rev. B **24**, 7275 (1981).

<sup>21</sup>R. T. Girard, O. Tjernberg, G. Chiaia, S. Soderholm, U. O. Karlsson, C. Wigren, H. Nylén, and I. Lindau, Surf. Sci. **373**, 409 (1997).

<sup>22</sup>S. H. Wei and A. Zunger, J. Cryst. Growth **86**, 1 (1988).

<sup>23</sup>S. H. Wei and A. Zunger, Phys. Rev. B **37**, 8958 (1988).

<sup>24</sup>S. H. Wei and A. Zunger, J. Vac. Sci. Technol. A **6**, 2597 (1988).

<sup>25</sup>W. Goepel, J. Pollmann, I. Ivanov, and B. Reihl, Phys. Rev. B **26**, 3144 (1982).

<sup>26</sup>D. Vogel, P. Kruger, and J. Pollmann, Phys. Rev. B **52**, 14 316 (1995).

<sup>27</sup>D. Vogel, P. Kruger, and J. Pollmann, Phys. Rev. B **54**, 5495 (1996).

<sup>28</sup>O. Madelung, M. Schulz, and H. Weiss, in *Semiconductors: Physics of II-VI and I-VII Compounds, Semimagnetic Semiconductors Science and Technology*, Landolt-Bornstein, New Series, Group III, Vol. 17b (Springer, Berlin, 1982).

<sup>29</sup>Y. Dou, R. G. Egdell, T. Walker, D. S. L. Law, and G. Beamson, Surf. Sci. **398**, 241 (1998).

<sup>30</sup>Y. Dou, T. Fishlock, R. G. Egdell, D. S. L. Law, and G. Beamson, Phys. Rev. B **55**, 13 381 (1997).

<sup>31</sup>I. Hamberg, C. G. Granqvist, K. F. Berggren, B. E. Sernelius, and L. Engstroem, Phys. Rev. B **30**, 3240 (1984).

<sup>32</sup>G. Sanon, R. Rup, and A. Mansingh, Phys. Rev. B **44**, 5672 (1991).

<sup>33</sup>R. L. Weiher and R. P. Ley, J. Appl. Phys. **37**, 299 (1966).

<sup>34</sup>I. Tanaka, M. Mizuno, and H. Adachi, Phys. Rev. B **56**, 3536 (1997).

<sup>35</sup>H. Odaka, S. Iwata, N. Taga, S. Ohnishi, Y. Kaneta, and Y. Shigesato, Jpn. J. Appl. Phys. **36**, 5551 (1997).

<sup>36</sup>E. A. Albanesi, S. J. Sferco, I. Lefebvre, G. Allan, and M. Lannoo, Solid State Commun. **86**, 27 (1993).

<sup>37</sup>M. Orita, H. Sakai, M. Takeuchi, Y. Yamaguchi, T. Fujimoto, N. Fukumoto, and I. Kojima, Hyomen Kagaku **17**, 440 (1996).

<sup>38</sup>T. L. Barr and Y. L. Liu, J. Phys. Chem. Solids **50**, 657 (1989).

<sup>39</sup>J. Robertson, J. Phys. C **12**, 4767 (1979).

<sup>40</sup>J. L. Jacquemin, C. Alibert, and M. DeMurcia, Phys. Solid State **51**, K75 (1972).

<sup>41</sup>K. C. Mishra, K. H. Johnson, and P. C. Schmidt, Phys. Rev. B **51**, 13 972 (1995).

- <sup>42</sup>D. Frohlich, R. Kenklies, and R. Helbig, *Phys. Rev. Lett.* **41**, 1750 (1978).
- <sup>43</sup>P. M. A. Sherwood, *Phys. Rev. B* **41**, 10 151 (1990).
- <sup>44</sup>N. I. Medvedeva, V. P. Zhukov, M. Y. Khodos, and V. A. Gubanov, *Phys. Status Solidi B* **160**, 517 (1990).
- <sup>45</sup>S. Munnix and M. Schmeits, *Phys. Rev. B* **27**, 7624 (1983).
- <sup>46</sup>R. G. Egdell, J. Rebane, T. J. Walker, and D. S. L. Law, *Phys. Rev. B* **59**, 1792 (1999).
- <sup>47</sup>L. Kover, G. Moretti, Z. Kovacs, R. Sanjines, I. Csemy, G. Margaritondo, J. Palinkas, and H. Adachi, *J. Vac. Sci. Technol. A* **13**, 1382 (1995).
- <sup>48</sup>J. M. Themlin, R. Sporcken, J. Darville, R. Caudano, J. M. Gilles, and R. L. Johnson, *Phys. Rev. B* **42**, 11 914 (1990).
- <sup>49</sup>J. M. Themlin, M. Chtaib, L. Henrard, P. Lambin, J. Darville, and J. M. Gilles, *Phys. Rev. B* **46**, 2460 (1992).
- <sup>50</sup>J. Chouvin, J. Olivier-Fourcade, J. C. Jumas, B. Simon, P. Bien-san, F. J. F. Madrigal, J. L. Tirado, and C. P. Vicente, *J. Electroanal. Chem.* **494**, 136 (2000).
- <sup>51</sup>I. Hamberg and C. G. Granqvist, *J. Appl. Phys.* **60**, R123 (1986).
- <sup>52</sup>A. K. Kulkarni and S. A. Knickerbocker, *J. Vac. Sci. Technol. A* **14**, 1709 (1996).
- <sup>53</sup>H. Odaka, Y. Shigesato, T. Murakami, and S. Iwata, *Jpn. J. Appl. Phys.* **40**, 3231 (2001).
- <sup>54</sup>O. N. Mryasov and A. J. Freeman, *Phys. Rev. B* **64**, 233111 (2001).
- <sup>55</sup>J. C. C. Fan and J. B. Goodenough, *J. Appl. Phys.* **48**, 3524 (1977).
- <sup>56</sup>V. Christou, M. Etchells, O. Renault, P. J. Dobson, O. V. Salata, G. Beamson, and R. G. Egdell, *J. Appl. Phys.* **88**, 5180 (2000).
- <sup>57</sup>R. G. Egdell, T. J. Walker, and G. U. Beamson, *J. Electron Spectrosc. Relat. Phenom.* **128**, 59 (2003).